Raji *et al.*
Journal of Engineering and Applied Science (2024) 71:40
https://doi.org/10.1186/s44147-024-00379-w

Journal of Engineering and Applied Science

RESEARCH **Open Access**

Channel estimation and MIMO combining architecture in millimeter wave cellular system with few ADC bits

Akeem Abimbola Raji[1*], Joseph Folorunso Orimolade[2], Kamoli Akinwale Amusa[3] and Isaiah Adediji Adejumobi[3]

*Correspondence: rajiakeemabimbola@gmail.com

[1] Department of Electrical and Electronics Engineering, College of Engineering and Environmental Studies, Olabisi Onabanjo University, Ibogun Campus, Ibogun, Ogun State, Nigeria
[2] Department of Electrical and Electronics Engineering, Caristas Institute of Higher Education, Hong Kong, Hong Kong
[3] Department of Electrical and Electronics Engineering, Federal University of Agriculture, Abeokuta, Nigeria

Abstract

Hybrid combiner and precoder architectures, radio frequency (RF) chain, analog phase shifters, digital-to-analog converter (DAC), and analog-to-digital converter (ADC) are components of a millimeter wave cellular system. Prior works in the area of millimeter wave cellular system design employ receiver with infinite bit and large amount of RF chain that scales linearly with the quantity of transmitting and receiving antennas. This mode of design no doubt increases power demand or requirement of a typical millimeter wave system. In this work, hybrid architecture with few RF chains and small number of ADC bits are proposed and are used as candidate for millimeter wave channel estimation and cellular communication. In that connection, least square (LS), orthogonal matching pursuit (OMP), compressed sampling matching pursuit (CoSAMP), and deep learning (DL) techniques are utilized for analytical investigation. Indeed, computational results reveal that, when ADC consisting of uniform mid- rise quantizer is employed, the performance of 4 and 6 bits at signal-to-noise ratio (SNR) values of − 10 dB and 20 dB is at par with infinite bit (unquantized case). As a validation, DL compares favorably well with adaptive compressed sensing (ACS) technique previously used in the literature for channel estimation, while OMP and CoSAMP show better performance than ACS.

Keywords: Analog-to-digital converter, Analog precoder and combiner, Baseband precoder and combiner, Channel estimation, Millimeter wave communication

Introduction

Increasing mobile traffic volume and spectrum shortage of traditional microwave cellular network have highlighted the need to consider large spectrum in millimeter wave band for communication where hybrid precoding and combining architectures cascaded with RF chain and ADC as well as DAC are utilized at the receiver and the transmitter. Previous research investigations have assumed hybrid precoder and combiner designs with large number of RF chains that is equivalent to the size of transmitting and receiving antennas and receiver with infinite bit [1–10]. A millimeter wave cellular system requires large number of antenna arrays for directional transmission and for the reduction of path loss associated with such high frequency communication. Using RF chains that are equal to the amount of transmitting and receiving antennas may not only increase hardware cost but also make the cellular system to be power hungry. An infinite bit receiver implies that the received signal is not quantized at mobile station. This does not conform to modern communication architecture design which has low resolution ADC as an important component of receiver architecture for transforming analog received signal-to-digital format for further processing. Efficient hardware architectures with few RF chains and low resolution ($\leq$6 bits) ADC [11] are therefore necessary for low power millimeter wave cellular communication. Hence, this work designs a millimeter wave cellular system with small amount of RF chains and few number of ADC bits. Specifically, millimeter channel estimation problem is addressed whose solution yields channel state information (CSI) which is effected via OMP, LS, CoSAMP, and DL. To the best we can ascertain, the use of CoSAMP and DL for obtaining CSI in a millimeter wave system with few ADC bits is receiving attention here for the first time.

Other research works reported in the literature include [12–15] which focus on estimation of channel characteristics in multiple input multiple output (MIMO) system with 1-bit ADC receiver, wherein no aspect of millimeter wave problem is addressed.

In article [16], authors propose modified expectation–maximization (EM) and generalized approximate passing (GAMP) algorithms for estimating millimeter wave channel in MIMO system with 1-bit quantization. The two methods require long training sequence to converge. In [17], authors consider millimeter wave system with few ADC bits, but it is assumed that the receiver and the transmitter have perfect information about the channel which is not realistic in practical sense.

In article [18], a combination of EM, Stein's unbiased risk estimate (SURE), and GAMP (EM-SURE-GAMP) is utilized for millimeter wave channel estimation using 1, 2, and 3 bits at the receiver. It is assumed that the amount of RF chain is equal to the quantity of antennas at base station and mobile station.

Authors in [19] consider ACS for channel estimation using receiver with 1 bit, which performs poorly in noisy SNR values, while authors in [20, 21] estimate uplink channel in a MIMO system whose base station utilizes 1 and 2 bits at the ADC and spatial sigma delta architecture.

Overall, the following contributions are made in this paper:

(1) A hybrid millimeter wave architecture with small amount of RF chains and few ADC bits are proposed for millimeter wave channel estimation and cellular communication.
(2) By using sparse property of millimeter wave channel, quantized millimeter wave channel estimation problem is formulated.
(3) CoSAMP and DL estimators are proposed for solving the quantized problem.
(4) As a validation, the methods are compared with models existing in the literature.

Notations: A scalar variable is represented by d, column vector is denoted by bold letter $\mathbf{d}$, and $\mathbf{D}$ is a matrix. $(\mathbf{D})^H$, $(\mathbf{D})^T$, $\|\mathbf{D}\|_F$ and $(\mathbf{D})^{-1}$ indicate, respectively, conjugate transpose of $\mathbf{D}$, transpose of $\mathbf{D}$, Frobenius norm of $\mathbf{D}$, and inverse of $\mathbf{D}$. $(\mathbf{D})^*$ represents conjugate of $\mathbf{D}$, and $vec(\mathbf{D})$ is the vector form of $\mathbf{D}$. The Euclidean norm of column vector $\mathbf{d}$ is represented by $\|\mathbf{d}\|_2$, while the absolute value of d is symbolized by $|d|$. $\otimes$ is the symbol for Kronecker product, and $diag(\mathbf{D})$ represents block diagonal matrix. $M \times M$ identity matrix is represented by I_M, and $\mathrm{N}(f,k)$ is the complex Gaussian random vector whose mean and covariance are f and k. E is the expectation operator, $\cdots$. is the ellipsis operator which indicates continuation of an equation, while $[\mathbf{D}]_{\mathrm{m,n}}$ denotes (m,n) -th entry of $\mathbf{D}$.

The rest of the paper is organized in such a way that the system model is described in the "Methods" section, discussion of simulation results is presented in the "Results and discussion" section, while concluding remarks are given in the "Conclusion" section.

Methods

Figure 1 illustrates downlink millimeter wave cellular system with few ADC bits at mobile station (MS). The base station (BS) consists of N_T antennas and F_T^{RF} RF chain to up convert spatial streams B_s to the carrier frequency. The baseband precoder at BS multiplexes the spatial streams which are attached to the transmitting antennas via analog phase shifter. The receiving MS receives the transmitted streams via N_R antennas. The analog combiner at MS digitally controls the amplitude and phase of the transmitted spatial streams. These are down-converted to carrier frequency using F_T^{RF} RF chain. ADC is used to transform the received analog signal to digital format for further processing by the digital combiner.

The received signal at MS after quantization and combining assumes expression of the form:

$$x = Q_{BB}^H \mathbb{Q}\left(Q_{Rf}^H H P_{RF} P_{BB} t + Q_{Rf}^H s\right) \tag{1}$$

in which x is the quantized received signal, $\mathbb{Q}(\cdot)$ is the quantization operator, $P_{RF} \in \mathbb{C}^{N_T \times F_T^{RF}}$ is RF precoding matrix, and $P_{BB} \in \mathbb{C}^{F_T^{RF} \times B_s}$ is the digital precoding matrix. $Q_{RF} \in \mathbb{C}^{N_R \times F_R^{RF}}$ and $Q_{BB} \in \mathbb{C}^{F_R^{RF} \times B_s}$, respectively, denote RF and baseband combining matrices, while $t \in \mathbb{C}^{B_s \times 1}$ is the transmitted symbol vector whose covariance matrix satisfies $E\left[tt^H\right] = \frac{I}{B_s}$. $s \in \mathbb{C}^{N_R \times 1}$ is the additive white Gaussian noise (AWGN) that distorts the received signal. $H \in \mathbb{C}^{N_T \times N_R}$ is the sparse millimeter wave channel of the form given by [5, 22, 23] as follows:

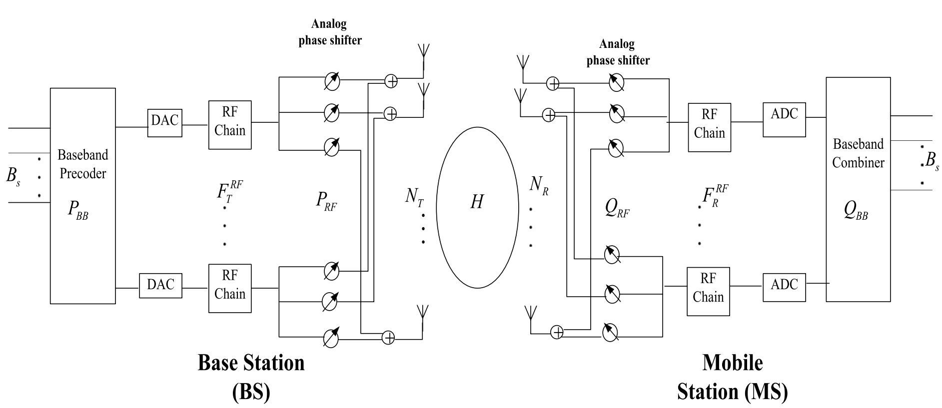

Fig. 1 Millimeter-wave hybrid precoding and combining system

$$H = \sqrt{\frac{N_T N_R}{K}} \sum_{k=1}^{K} \rho_k f_R(\theta_k) f_T^H(\varphi_k) \quad (2)$$

in which $K \ll \min(N_T, N_R)$ is the channel path between BS and MS, ρ_k is the complex gain associated with k^{th} path, and $f_R(\theta_k)$ and $f_T(\varphi_k)$ represent array steering vectors at MS and BS. θ_k and φ_k are azimuth angle of arrival (AoA) at MS and azimuth angle of departure (AoD) from BS.

If the transmitting BS and receiving MS consist of uniform linear antenna arrays, then array steering vectors are expressible in forms given by Eq. (3) [24].

$$f_T(\varphi_k) = \sqrt{\frac{1}{N_T}} \left[1, e^{j\frac{2\pi}{\lambda}d_a \sin(\varphi_k)}, e^{j\frac{4\pi}{\lambda}d_a \sin(\varphi_k)}, \ldots, e^{j(N_T-1)\frac{2\pi}{\lambda}d_a \sin(\varphi_k)}\right]^T \quad (3a)$$

$$f_R(\theta_k) = \sqrt{\frac{1}{N_R}} \left[1, e^{j\frac{2\pi}{\lambda}d_a \sin(\theta_k)}, e^{j\frac{4\pi}{\lambda}d_k \sin(\theta_k)}, \ldots, e^{j(N_R-1)\frac{2\pi}{\lambda}d_a \sin(\theta_k)}\right]^T \quad (3b)$$

wherein λ is the wavelength and $d_a = \lambda/2$ is the spacing between antenna array elements.

Equation (2) assumes virtual representation as follows:

$$H = F_R(\alpha) F_T^H \quad (4)$$

where $\alpha = \sqrt{\frac{N_T N_R}{K}} \, diag \, [\rho_1, \rho_2, \ldots, \rho_k]^T$ is a diagonal matrix with path gain ρ_k. F_R and F_T are array response matrices given by Eq. (5) as follows:

$$F_R = [f_R(\theta_1), f_R(\theta_2), \ldots, f_R(\theta_K)] \in \mathbb{C}^{N_R \times K} \quad (5a)$$

$$F_T = [f_T(\varphi_1), f_T(\varphi_2), \ldots, f_T(\varphi_K)] \in \mathbb{C}^{N_T \times K} \quad (5b)$$

Neglecting grid quantization error, it is expected that H is equal to estimated quantized counterpart represented by $\bar{H}^q$ which consists of discretized AoA and AoD. This implies the following:

$$\bar{H}^q = \bar{F}_R(\gamma) \bar{F}_T^H \quad (6)$$

$\bar{F}_R$, $\bar{F}_T$ are array steering matrices with AoA and AoD taken from discretized grids of sizes P_R, P_T, respectively, and γ is the K-sparse matrix containing the channel gain.

For the purpose of estimating parameters in (6), the transmitter sends identical symbol t_m using $V_m \in \mathbb{C}^{N_T \times M}$ training precoder during M time instant, while the mobile station employs $G_m \in \mathbb{C}^{N_R \times F_R^{RF}}$ combiner to construct the received signal as Eq. (7) [25].

$$z_m = \mathbb{Q}\left(\sqrt{\wp}\, G_m^H \bar{H}^q V_m + G_m^H s_m\right) \quad (7)$$

in which $\wp$ is the average received power and $m = 1, \ldots, M$ is the number of training sequences.

Representation of Eq. (7) in vector form by using vector identity, $vec(ABC) = C^T \otimes A \, vec(B)$, leads to Eq. (8) given by the following:

$$z = \mathbb{Q}\left(\left(\sqrt{\wp}\left(V_m^T \otimes {G_m}^H\right) vec\left[\bar{H}^q\right] + w\right)\right) \tag{8}$$

in which z is the vectorized quantized received signal and $w = \ diag\left[{G_m}^H vec(s_m)\right]$ is the noise vector.

Substitution of Eq. (6) in Eq. (8) leads to an expression of the form:

$$z = \mathbb{Q}\left(\left(\sqrt{\wp}\left({V_m}^T \otimes {G_m}^H\right)\left(\bar{F}_T^* \otimes \bar{F}_R\right) vec(\gamma) + w\right)\right) \tag{9}$$

V_m and G_m in Eq. (9) are constructed with random entries expressed by Eq. (10) [9] as follows:

$$[V]_{i,k} = \frac{1}{\sqrt{N_T}} e^{j\frac{k_Q 2\pi}{2^{N_q^T}}} \tag{10a}$$

$$[G]_{i,k} = \frac{1}{\sqrt{N_R}} e^{j\frac{k_R 2\pi}{2^{N_q^R}}} \tag{10b}$$

where $k_Q = 0, 1, 2, \ldots, 2^{N_q^T} - 1$ and $k_R = 0, \ 1, \ 2, \ldots, 2^{N_R^T} - 1$, with N_q^T, N_q^R, indicating quantization bits in the phase shifter at BS and MS, respectively.

Equation (9) may be written in a form given as follows:

$$z = \mathbb{Q}\left(\sqrt{\wp}\,\Phi\, y + w\right) \tag{11}$$

in which $\Phi = \left({V_m}^T \bar{F}_T^* \otimes \bar{F}_R \ {G_m}^H\right)$ is the sensing matrix and $y = vec(\gamma)$ is the unknown sparse channel gain.

Equation (11) is the quantized sparse problem whose only unknown is the channel gain. For solving the sparse problem, uniform mid-rise quantizer that is symmetrical about the origin with quantization step size $\Delta \ = f\Big/2^{g-1}$ is utilized, in which f is expressed by the following:

$$f = \max \ abs\{\Re(z), \ \Im(z)\} \tag{12}$$

wherein $\Re(z)$, $\Im(z)$ are, respectively, real and imaginary parts of quantized received signal, while g is the number of bits in ADC. The channel gain is obtained via quantized versions of CoSAMP and OMP algorithms presented in the subsequent sections.

On the other hand, when infinite bit is invoked, Eq. (13) emerges which is the unquantized version of Eq. (11) which assumes expression of the form:

$$r = \sqrt{\wp}\,\Phi\, y + w \tag{13}$$

in which r is unquantized received signal and other parameters remain as defined earlier.

Compressed sampling matching pursuit solution

Algorithm 1 Compressed matching pursuit

1: **Inputs**: Sensing matrix $\mathbf{\Phi}$, measurement vector $\boldsymbol{z}$, and sparsity K
2: **Initials:** $\boldsymbol{y}_0 = 0,\ \boldsymbol{r} = \boldsymbol{z},\ T = \varnothing$
3: **Repeat**
4: $i = 1;\ \ i = i + 1$
5: $\boldsymbol{p} = |\langle\ \mathbf{\Phi},\ \boldsymbol{r}_{i-1}\rangle|$
6: $\Gamma =$ supp $(\boldsymbol{p}_{2K})$
7: $\Omega = \Gamma \bigcup T\ \rightarrow$
8: $\boldsymbol{y}_i = argmin\left\|\boldsymbol{r}_{i-1} - \sqrt{\wp}\,\Phi_\Omega\,\boldsymbol{y}_i\right\|_2^2$
9: $\boldsymbol{y}_i = \boldsymbol{y}_K$
10: $r_i = \boldsymbol{z} - \sqrt{\wp}\,\mathbf{\Phi}\,\boldsymbol{y}_i\ \ \rightarrow$
11: Iterate from step 5 until norm of the residual is less than a threshold
12: **end for**
13: **Output:** r_i, and channel gain $\boldsymbol{y}_i$

Orthogonal matching pursuit solution

Algorithm 2 Orthogonal marching pursuit

1**: Inputs**: Sensing matrix Φ and measurement vector $\boldsymbol{z}$
2: **Initialize** $y_0 = 0,\ r_0 = \boldsymbol{z},\ T_0 = \varnothing$
3: **for** $i = 1;\ i = i + 1$, **do**
4: $\boldsymbol{p} = \underset{j=1,\ldots,K_T K_R}{arg\,max}\left|\langle\ \mathbf{\Phi}_j,\ \boldsymbol{r}_{i-1}\rangle\right|$
5: $T_i = T_{i-1} \bigcup \{\boldsymbol{p}\}$
6: $\boldsymbol{y}_i = argmin\left\|\boldsymbol{r}_{i-1} - \sqrt{\wp}\,\Phi_{T_i}\,\boldsymbol{y}_i\right\|_2^2$
7: $\boldsymbol{r}_i = \boldsymbol{z} - \sqrt{\wp}\,\Phi_{T_i}\boldsymbol{y}_i$
8: Iterate from step 4 until norm of residual is less than the threshold
9: **end for**
10: **Output:** r_i and channel gain $\boldsymbol{y}_i$

By invoking $\gamma = vec^{-1}\left(y\right)$ in Eq. (6), CSI emerges which facilitates the design of combiner architecture which is considered later in this work.

Deep learning (DL) channel estimation

Moreover, in solving the sparse problem of Eq. (11), a deep neural network is trained, consisting of input layer through which data sets enter the network, three hidden layers, and output layer. As illustrated in Fig. 2, multilayer perceptron (feed forward) network model is adopted, where sigmoid linear function and softmax function are

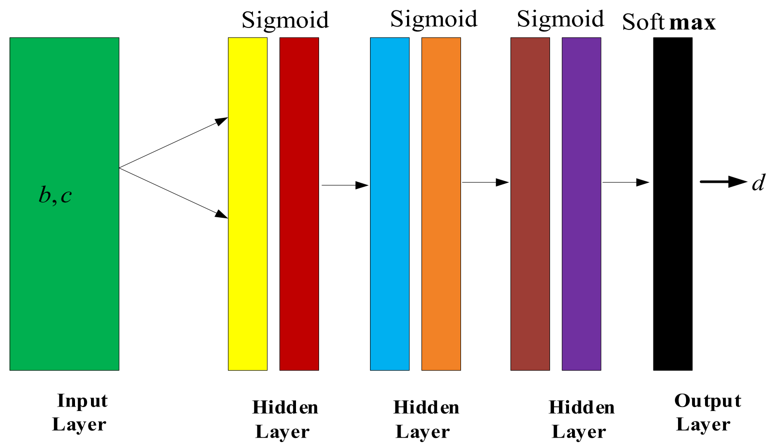

Fig. 2 Deep neural network for channel estimation

employed as activation functions at hidden and output layers, respectively. Given an input argument a, the sigmoid and softmax functions assume forms given as follows:

$$sigmoid(a) = \frac{1}{1+e^{-a}} \tag{14a}$$

$$soft\ \max(a) = \frac{e^{a}}{\sum e^{a}} \tag{14b}$$

The training data set consists of input c which is the correlation vector between the sensing matrix Φ and measurement vector z, and the target b, which is the channel amplitude of simulated millimeter wave environment. The target consists of $\mathbb{C}^{P_T \cdot P_R \times 1}$ entries as given by the following:

$$b = \left[\left|b(1)\right|, \left|b(2)\right|, \left|b(3)\right| \ldots, \left|b(P_T \times P_R)\right|\right]^T \in \mathbb{C}^{P_T P_R \times 1} \tag{15}$$

The output of the network, represented by d, is the estimated channel amplitude which is obtained via Eq. (16) as follows.

$$d = f(\Omega, w) \tag{16}$$

where $f(\cdot)$ is the mapping function, Ω is the training data set, and w is the weight of the deep neural network which is updated by using back propagation algorithm where the error or loss is given by Eq. (17) as follows:

$$Loss = \frac{1}{T}\sum_{n=1}^{T}\left\|b(n) - d(n)\right\|_2^2 \tag{17}$$

in which T is the number of iterations.

$|d|$ is sorted in descending manner to obtain the indices of the first h entries, where h represents the number of dominant entries in d and which corresponds to the sparsity level of simulated millimeter wave channel environment as used elsewhere [26].

The dominant entries of channel gain are obtained by plucking in the columns of the sensing matrix with dominant indices and solving problem of Eq. (18) given as follows:

$$y[J] = \left(\Phi_J^H \Phi_J\right)^{-1} \Phi_J^H z \tag{18}$$

where Φ_J is the sensing matrix consisting of J column indices with $J \in \mathbb{R}^h$.

Once the channel gain is known, DL channel estimate is determined by using Eq. (19), written as follows:

$$\bar{H}_{dl}^q = \bar{F}_R \, vec^{-1}(y) \, \bar{F}_T^H \tag{19}$$

wherein $\bar{H}_{dl}^q$ is the DL channel estimate.

The detailed procedure for obtaining channel gain and for constructing DL channel estimate is presented in Algorithm 3 below.

Algorithm 3 Deep learning channel estimation

1: **Inputs**: Sensing matrix $\boldsymbol{\Phi}$, measurement vector $\boldsymbol{z}$, and sparsity level K
2: **Initials**: $\boldsymbol{y}_0 = 0$
3: Generate randomly $\boldsymbol{b} \in \mathbb{C}^{P_T P_R \times 1}$ based on simulated millimeter wave channel characteristics and determine its absolute value
4: Train a DL network with datasets $\mathbf{c}, \boldsymbol{b}$ and deduce channel amplitude $\boldsymbol{d}$ and update the weight via back error propagation algorithm
5: Arrange the indices of $\boldsymbol{d}$ in descending order and obtain h dominant entries corresponding to sparsity of a millimeter wave channel
6: Deduce columns in sensing matrix Φ with corresponding dominant indices and compute $\boldsymbol{y}[J] = \left(\boldsymbol{\Phi}_J^H \boldsymbol{\Phi}_J\right)^{-1} \boldsymbol{\Phi}_J^H \boldsymbol{z}$ for $J \in \mathbb{R}^h$
7: **Output**: $\boldsymbol{y}$
8: Determine the deep learning channel estimate according to $\bar{\boldsymbol{H}}_{dl}^q = \bar{F}_{\boldsymbol{R}} \, vec^{-1}(\boldsymbol{y}) \bar{F}_{\boldsymbol{T}}^H$

Least square (LS) solution

The quantized LS channel model is expressible from Eq. (8) as follows:

$$z = \mathbb{Q}\left(\left(\sqrt{\wp}\left(V_m^T \otimes {G_m}^H\right) \bar{H}_{LS}^q + w\right)\right) \tag{20}$$

wherein $\bar{H}_{LS}^q$ is the quantized LS channel estimate that assumes expression of the form given as follows:

$$\bar{H}_{LS}^q = \frac{1}{\sqrt{\wp}} \left(B^H B\right)^{-1} B^H z \tag{21}$$

where $B = {V_m}^T \otimes {G_m}^H$

Hybrid combiner design

The millimeter wave CSI obtained from OMP, CoSAMP, and DL as well as LS is employed to design hybrid combiner by solving Frobenius problem of Eq. (22) in a manner similar to the one provided in [27].

$$(Q_{RF}, Q_{BB}) = \underset{Q_{RF}, Q_{BB}}{\arg\min} \left\| Q_{opt} - Q_{RF} Q_{BB} \right\|_F \text{subject to the following:}$$

$$|Q_{RF}| \in A_T \; and \; \|Q_{RF} Q_{BB}\|_F^2 = B_s \tag{22}$$

where $Q = Q_{RF} Q_{BB}$ is the combiner design. It is expected that Q is close to optimum unconstrained combiner, denoted by Q_{opt}, and which corresponds to left singular matrix of the quantized millimeter wave channel estimate $\bar{H}^q$. That is $Q_{opt} = U$, given that $\bar{H}^q = U D V^H$, where V is the right singular matrix. It is assumed that Q_{RF} is constrained to a set of array responses $X_T = [x_t(\varphi_1, \theta_1), x_t(\varphi_2, \theta_2), \ldots, x_t(\varphi_b, \theta_b)]$, with b being the angular resolution.

Results and discussion

The performance of OMP, CoSAMP, DL, and LS methods for quantized millimeter wave channel estimation and combiner design is evaluated. It is considered that $N_T = 64$, $N_R = 32$, $K = 7$, number of RF chains at BS and MS is 5, $N_q^T = N_q^R = 2$, frequency of operation is 32 GHz, system bandwidth is 500 MHz, and $M = 40$ [25]. $\bar{F}_T$ and $\bar{F}_R$ matrices are constructed with AoD and AoA uniformly distributed on discretized points $P_T = N_T$ and $P_R = N_R$. A geometric millimeter wave channel model H is constructed with AoA and AoD uniformly distributed over $(0, 2\pi)$, while the gain is Gaussian random variable, identically and independently distributed. Complex Gaussian random distribution with entries $\mathbb{N}(0, \sigma^2)$ is used to represent AWGN where $\sigma^2 = c_0 \, Bandwidth$ indicates total noise power and c_0 is the noise power density. The received power $\wp = SNR \, \sigma^2$, in which SNR is the signal-to-noise ratio in decibel. CoSAMP and OMP algorithms are terminated when norm of residual is less than 10^{-10}, i.e., $\|r\|_2 < 10^{-10}$ [25].

The DL neural network consists of single input layer, softmax output node, and three hidden layers, each with 512, 256 and 128 hidden sigmoid nodes. The network is trained over 1200 epochs with learning rate of 0.01 and 20% probability dropout of hidden neurons.

Normalized mean square error (NMSE) in decibel and spectral efficiency are used as performance indices and are expressed by Eqs. (23) and (24) as follows:

$$NMSE(dB) = 10 \log_{10} \left[\frac{\left\| H - \bar{H}^q \right\|_F^2}{\|H\|_F^2} \right] \tag{23}$$

$$\text{Spectral efficiency} = \log_2 \left| I_{B_s} + \frac{SNR}{B_s} \left(Q^H Q\right)^{-1} Q^H H P P^H H^H Q \right| \tag{24}$$

where all symbols remain as defined earlier.

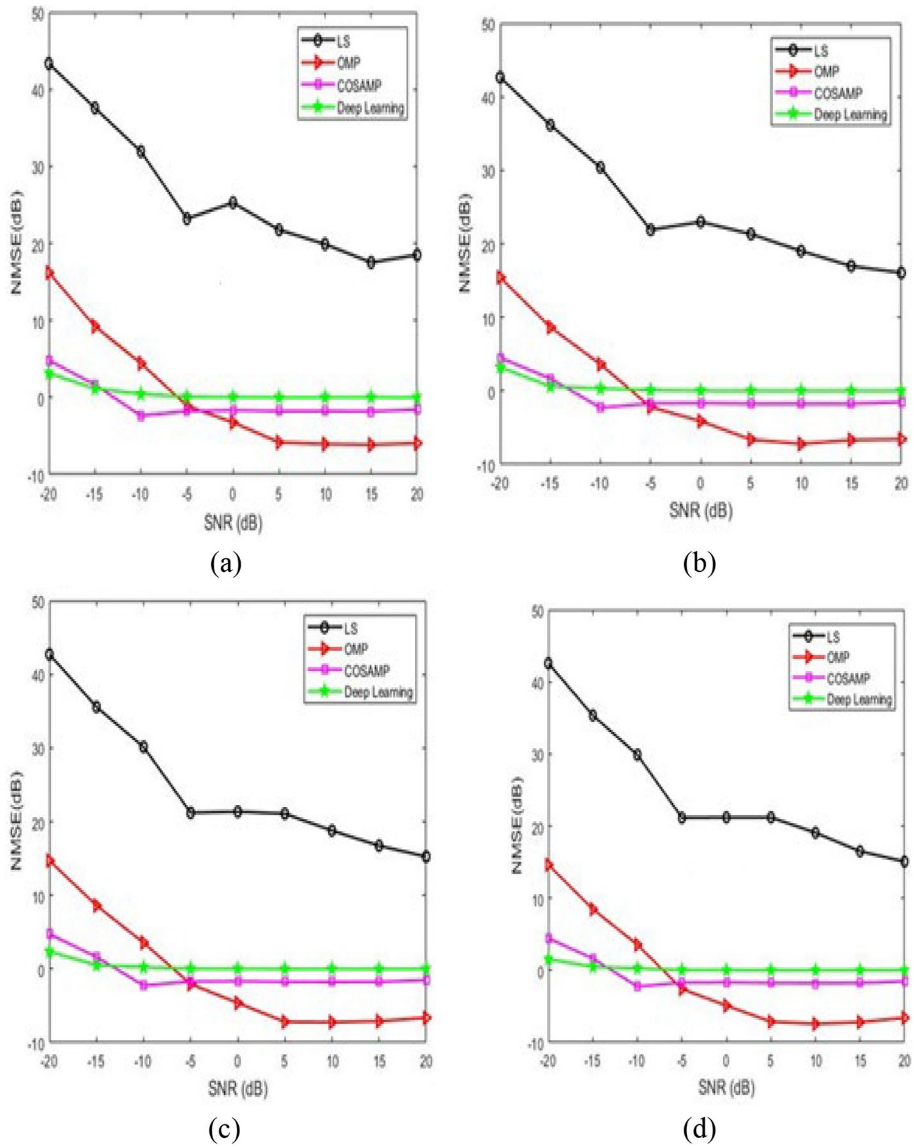

Fig. 3 NMSE versus SNR for LS, OMP, COSAMP, and DL using **a** 2 bit, **b** 3 bit, **c**, 4 bit, and **d** 6 bit

It is worthy to mention that while NMSE reveals the error in the utilization of LS, OMP, CoSAMP, and DL for channel estimation, spectral efficiency indicates the rate at which spatial stream B_s is transmitted from BS to MS with ADC. Figure 3 portrays response behavior of NMSE of OMP, CoSAMP, DL, and LS to variation of SNR from − 20 to 20 dB wherein the number of bits in ADC $g = 2, 3, 4$, and 6, respectively.

It is observed that LS exhibits the poorest behavior in all the results displayed in Fig. 3. This is in line with what has been consistently reported in the literature which is attributed to the inability of LS method to exploit the sparsity of millimeter wave channel for estimation. It is seen in Fig. 3a–d that OMP performs better than CoSAMP and DL when SNR is −5 dB and above, whereas CoSAMP and DL outperform OMP when SNR is below −5 dB.

Table 1 NMSE of LS, OMP, CoSAMP, and DL for 2, 3, 4, 6, and infinite bit

SNR(dB)									
	-20	**-15**	**-10**	**-5**	**0**	**5**	**10**	**15**	**20**
ADC bits	NMSE (dB) for LS								
Infinite	42.5159	35.3573	29.9541	21.1436	21.0443	21.1026	19.1538	16.4678	14.8914
2	43.3190	37.5576	31.9095	23.1951	25.2676	21.7531	19.8947	17.5118	18.5020
3	42.6157	36.1318	30.3873	21.9043	22.9805	21.3230	19.0149	16.9698	16.0480
4	42.6912	35.5571	30.1225	21.1948	21.3375	21.0678	18.7741	16.7218	15.2454
6	42.5771	35.3500	29.8977	21.1635	21.2097	21.2097	19.0711	16.5086	15.0763
NMSE (dB) for OMP									
Infinite	14.7068	8.6693	3.6425	-2.5419	-4.9715	-7.1623	-7.4314	-7.1858	-6.5818
2	16.2074	9.2391	4.4341	-1.0789	-3.3246	-5.8134	-6.0406	-6.1267	-5.9366
3	15.4232	8.6686	3.6225	-2.1872	-4.1170	-6.6021	-7.2015	-6.6603	-6.5540
4	14.6998	8.6054	3.6572	-2.0559	-4.6165	-7.1768	-7.2337	-7.0883	-6.6251
6	14.6364	8.470	3.5550	-2.5889	-4.8918	-7.1178	-7.4249	-7.1804	-6.5879
NMSE (dB) for CoSAMP									
Infinite	4.4097	1.5478	-2.2424	-1.7109	-1.6673	-1.7447	-1.7807	-1.7576	-1.5298
2	4.8346	1.6636	-2.3607	-1.7739	-1.6613	-1.7763	-1.7724	-1.8129	-1.5613
3	4.5107	1.6896	-2.2797	-1.7061	-1.6570	-1.7430	-1.7654	-1.7483	-1.5286
4	4.7273	1.6324	-2.2407	-0.17084	-1.6888	-1.7472	-1.7748	-1.7554	-1.5261
6	4.4463	1.6465	-2.2443	-1.7107	-1.6666	-1.7469	-1.7821	-1.7564	-1.5294
NMSE (dB) for DL									
Infinite	2.8343	0.7922	0.1988	0.0395	0.0216	0.0355	0.0303	0.0180	0.0166
2	3.1492	1.1588	0.4645	0.0776	0.0603	0.0164	0.0284	0.0312	0.0170
3	3.2380	0.6147	0.3343	0.1088	0.0281	0.0173	0.0106	0.0060	0.0153
4	2.3565	0.5187	0.2424	0.0426	0.0424	0.0155	0.0262	0.0175	0.0209
6	1.5489	0.5060	0.2750	0.0402	0.0233	0.0182	0.0249	0.0214	0.0231

However, Table 1 presents the values of NMSE for OMP, CoSAMP, DL, and LS when 2, 3, 4, 6, and infinite bits are used for all values of SNR employed as candidate for investigation in this work.

A cursory look at Table 1 reveals that the values of NMSE for CoSAMP, DL, LS, and OMP using infinite bit at SNR of − 10 dB are, respectively, −2.2424 dB, 0.1988 dB, 29.9541 dB, and 3.6425 dB, while those with 4 bit at − 10 dB are −2.2407 dB, 0.200 dB, 30.100 dB, and 3.5572 dB, respectively. This implies that 4 bit has close values of NMSE with those of infinite bit at SNR of − 10 dB. On the other hand, NMSEs of DL, CoSAMP, LS, and OMP using infinite bit at 20 dB are −1.5298 dB, 0.0166 dB, 14.8914 dB, and − 6.5818 dB, respectively, whereas those for 6-bit are −1.5294 dB, 0.0231 dB, 15.0763 dB, and − 6.5879 dB, respectively, which indicates also that ADC with 6-bit resolution has close values of NMSE as those of infinite bit at SNR of 20 dB.

By employing Eq. (24), where it is assumed that BS utilizes unconstrained precoder and MS utilizes ADC with $g = 2, 3, 4$ and 6 bit respectively, Fig. 4 illustrates the characteristic profile of spectral efficiency against SNR. It is noticed in all the results depicted in Fig. 4 that spectral efficiency rises with increase in SNR. The implication of which is that spectral efficiency increases as noise reduces in the channel which is consistent with what is expected.

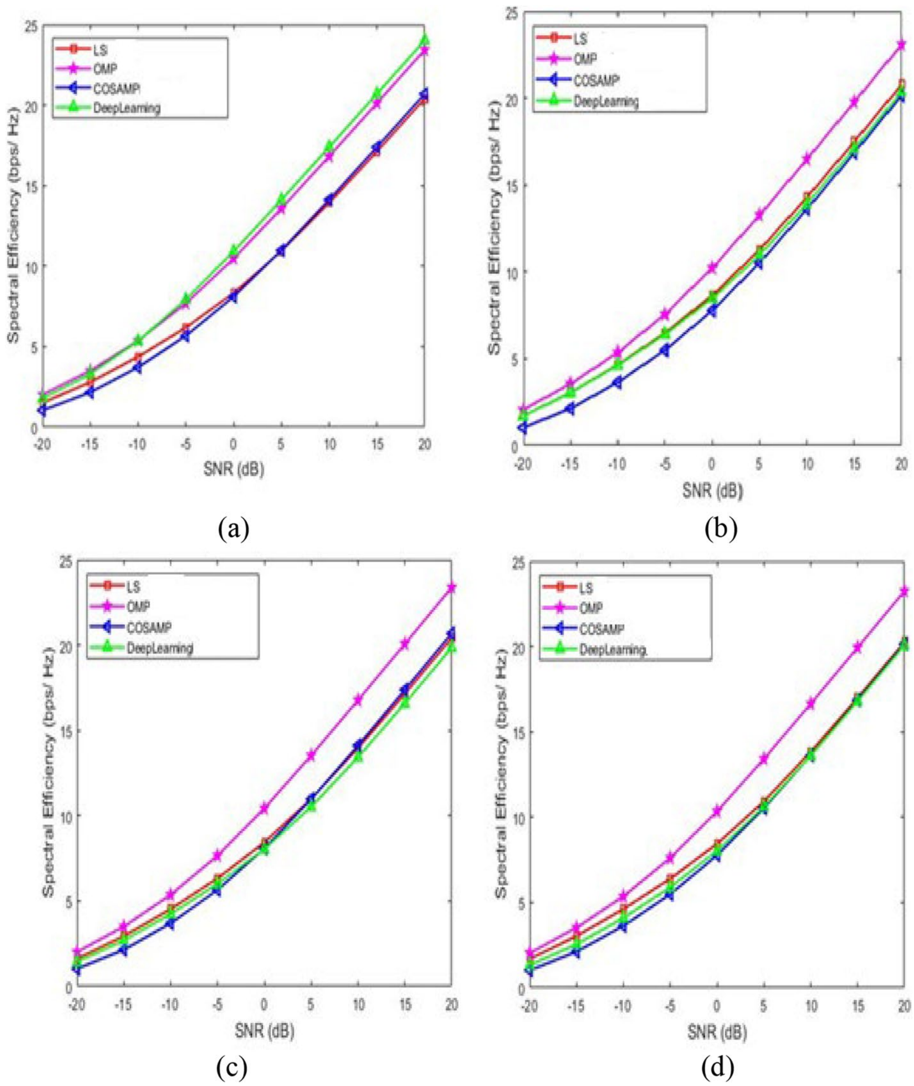

Fig. 4 Spectral efficiency against SNR for LS, OMP, COSAMP, and DL using **a** 2 bit, **b** 3 bit, **c** 4 bit, and **d** 6 bit

In Fig. 4a, it is observed that DL has the highest spectral efficiency when the receiver utilizes 2-bit and is closely followed by OMP, while for 3, 4, and 6 bits, OMP has the highest spectral efficiency as evidenced in Fig. 4b–d.

Effect of varying RF chain on NMSE and spectral efficiency

Figure 5 typifies graphical illustrations of response of NMSE to variation of SNR from − 20 to 20 dB wherein RF chains at the receiver and transmitter are 4, 6, 8, and 10, respectively, while using 4 bit at MS.

It is evident in Fig. 5 a and b that LS exhibits the worst performance over SNR of − 20 to 20 dB. It is however observed in Fig. 5d that LS improves drastically and has lower error than others when SNR is above 7 dB which indicates that the increase in amount of RF chain impacts positively on the performance of LS. The results in Fig. 5 also show that OMP performs better than CoSAMP when SNR is above − 6 dB, while below − 6 dB,

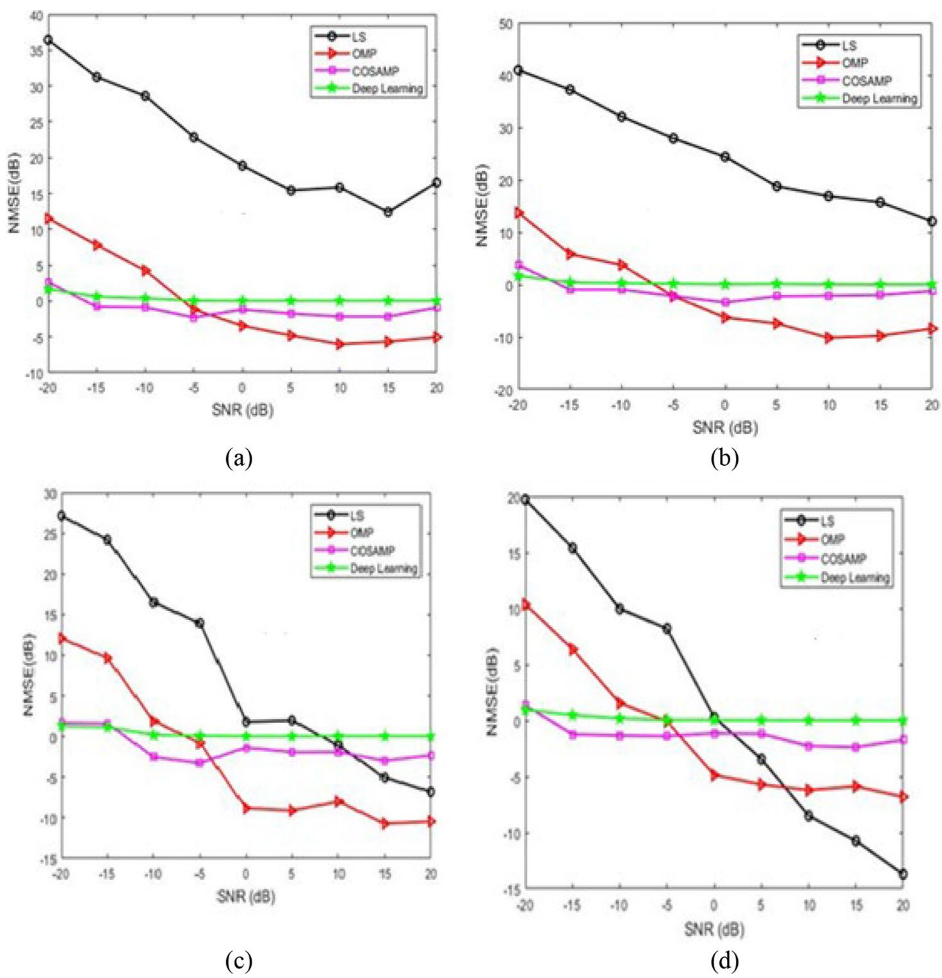

Fig. 5 NMSE against SNR for LS, OMP, CoSAMP, and DL with 4 bit and number of RF chains at the receiver and transmitter is **a** 4, **b** 6, **c** 8, and **d** 10

CoSAMP has lower errors than OMP. DL however outperforms OMP when SNR is below − 5 dB.

Figure 6 typifies spectral efficiency against SNR of all the channel estimation methods by using 4 bit and 4, 6, 8, and 10 RF chains at MS and BS. It is noticed in Fig. 6 that spectral efficiency increases with SNR. Furthermore, DL has the highest spectral efficiency in Fig. 6a, where 4 RF chains are utilized. OMP has better spectral efficiency when 6, 8, and 10 RF chains are utilized as observed in Fig. 6 b − d.

Effect of varying channel path on NMSE and spectral efficiency

Figure 7 depicts computational results for NMSE of LS, OMP, CoSAMP, and DL against SNR, where K varies from 4 to 10 and by employing 4-bit ADC at the receiver.

It is observed in Fig. 7 that the performance of OMP is better than other methods at higher values of SNR. LS exhibits the worst performance in all cases considered.

In Fig. 8a − d, it is seen that spectral efficiency increases with SNR for all the channel paths considered with OMP exhibiting the highest spectral efficiency when $K = 4$ and 6,

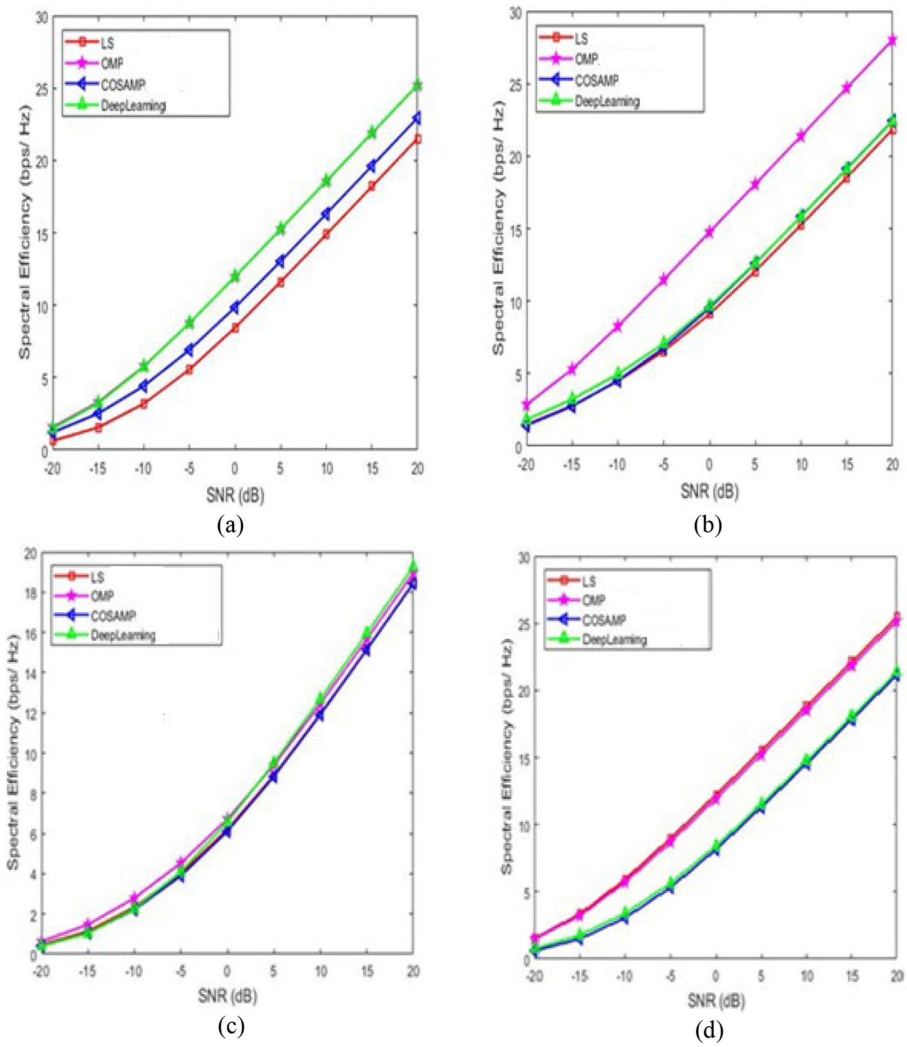

Fig. 6 Spectral efficiency versus SNR for LS, OMP, CoSAMP, and DL with 4-bit ADC, and number of RF chains at the receiver and transmitter is **a** 4, **b** 6, **c** 8, and **d** 10

while DL outperforms others when more channel paths of $K = 8$ and 10 are introduced into the design.

Validation

Here, the performance of OMP, CoSAMP, DL, and LS is compared with ACS of [23] existing in the literature. In the said work, hierarchical multi-resolution beam-forming vector is built for the training precoding and combining vector. And to facilitate computational evaluation with ACS, a millimeter-wave cellular system equipped with $N_T = 64$ and $N_R = 32$, operating at 32 GHz, is considered. The number of quantization bits employed at the phase shifter is 7, in order to be consistent with what is done in the publication. An infinite bit is employed in all the simulation data obtained here as there is no indication of quantization of the received signal at MS in the published work. The number of beam-forming vectors for ACS and training overhead (M) for implementing LS, OMP, CoSAMP, and DL are 32.

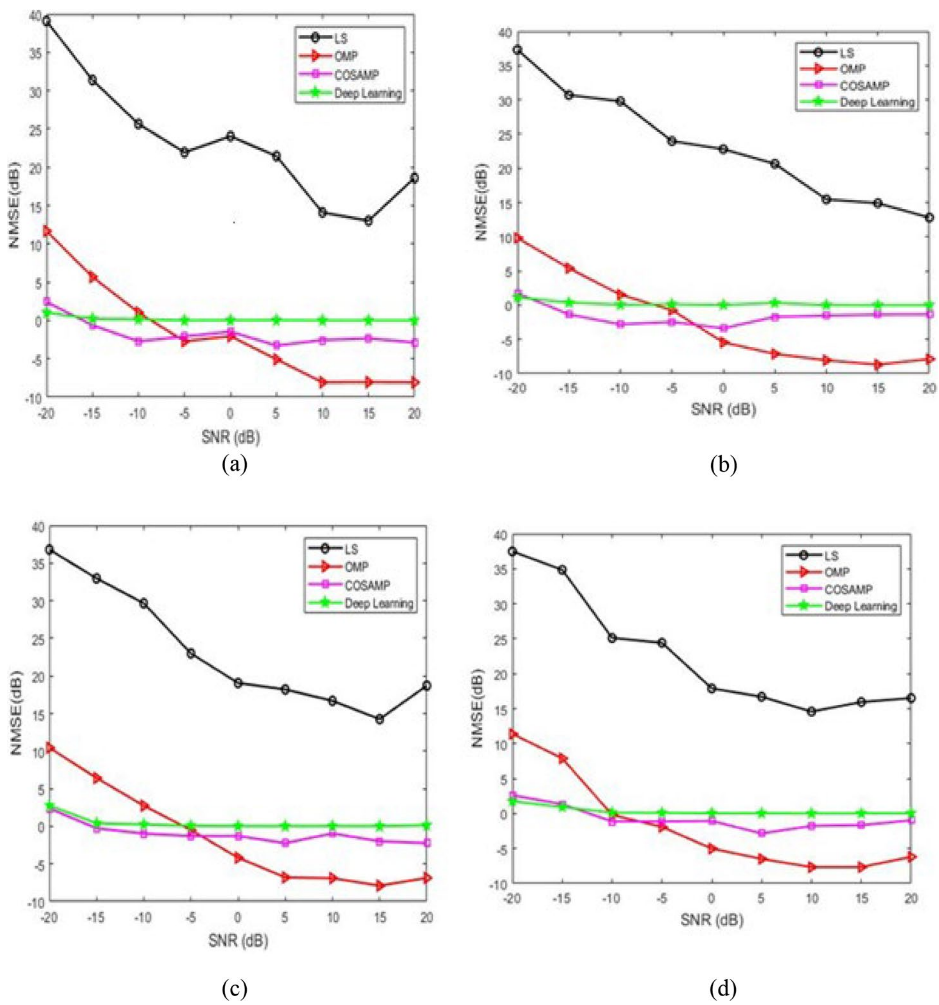

Fig. 7 NMSE versus SNR for LS, OMP, CoSAMP, and DL using 4-bit ADC, and the number of channel paths is **a** 4, **b** 6, **c** 8, and **d** 10

In addition, the number of uniform grid point assumed for ACS is 64, quantized grids employed in LS, OMP, CoSAMP, and DL are $P_T = N_T$ and $P_R = N_R$, while $K = 2$. Figure 9 compares NMSE of LS, OMP, CoSAMP, DL, and ACS where RF chains at BS and MS are set as 4 and 6.

In obtaining simulation results for ACS, simulation code provided by authors [28] is utilized. It is seen in the results displayed in Fig. 9 that LS exhibits the worst performance across SNR regime of − 20 to 20 dB. It is also observed that DL and ACS are at par in the two cases considered. Furthermore, it is observed in Fig. 9a that CoSAMP is better than ACS within SNR range of − 10 to 20 dB. OMP is better than ACS within SNR range of − 5 to 20 dB which is consistent with what is reported by [2].

However, it is noticed in Fig. 9b that the range of SNR for which the NMSE of CoSAMP is better than ACS increases when RF chain increases to six.

Figure 10 compares spectral efficiency of analytical models used in this work with that of ACS using 4 and 6 RF chains. It is evident in Fig. 10a and b that spectral efficiency of OMP is higher than those of CoSAMP, DL, LS, and ACS. It is also

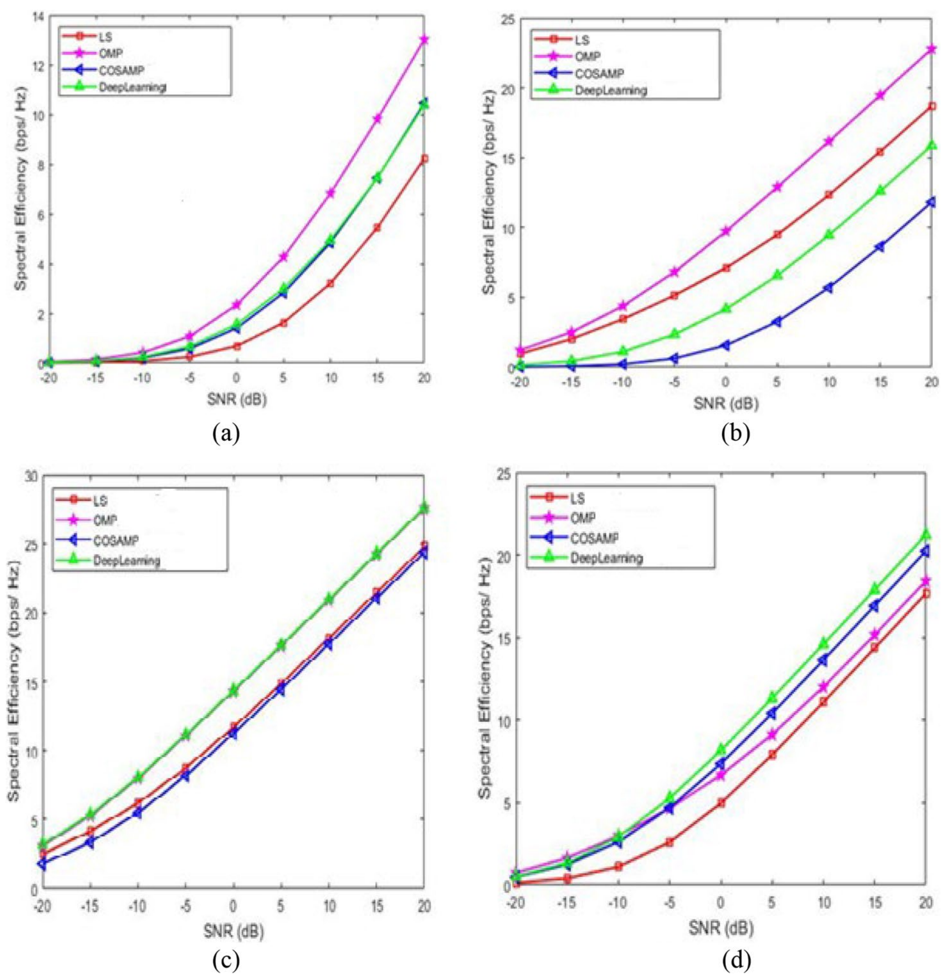

Fig. 8 Spectral efficiency against SNR for LS, OMP, CoSAMP, and DL channel using 4-bit ADC and **a** $K=4$, **b** $K=6$, **c** $K=8$, and **d** $K=10$

observed in Fig. 10a that spectral efficiency of CoSAMP is better than that of ACS in the SNR regime of − 20 to 15 dB, and the performance gap between CoSAMP and ACS widens when 6 RF chains are utilized as observed in Fig. 10b.

In terms of computational complexity, LS requires $O\ (MF_R{}^{R_f} N^2{}_T N^2{}_R)$ computational operations, resulting from matrix multiplication of B^H and B in Eq. (21). The computational complexity of OMP and CoSAMP having the same stopping criterion scales as $O\left(MF_R{}^{R_f}\, P_T\ P_R\right)$ and which results from the inner product of quantized received signal z and sensing matrix Φ [25]. The complexity of DL is based upon the number of epochs used for training the weight. For ACS, the computational complexity is $O\left(2K\,N_T^3\ \log_{\,t}\left(K_{AM}/K\right)\right)$ [29], where t and K_{AM} are, respectively, numbers of beam-forming vector, and quantized grid and other quantities remain as defined earlier. It is therefore seen that LS has the highest computational operation, closely followed by ACS, while DL is implemented with the least computational effort and has computational edge over OMP and CoSAMP.

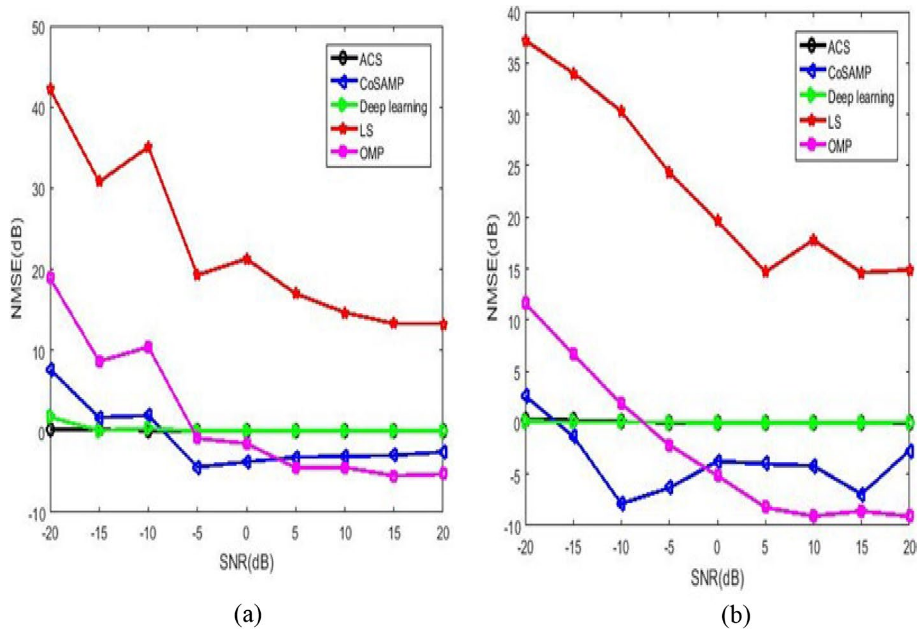

Fig. 9 NMSE against SNR for LS, OMP, CoSAMP, DL, and ACS, and the number of RF chains is **a** 4 and **b** 6

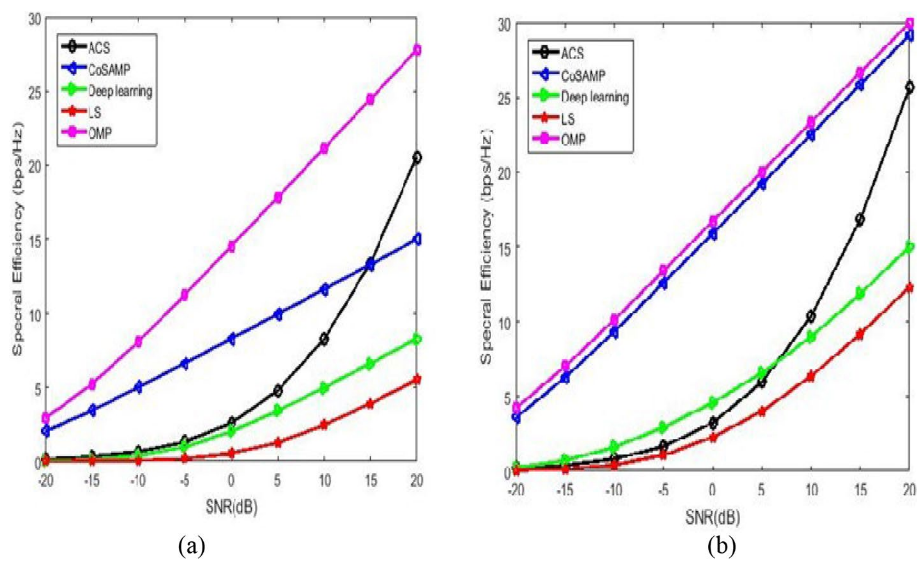

Fig. 10 Comparison of spectral efficiency of LS, OMP, CoSAMP, DL, and ACS for **a** 4 RF chains and **b** 6 RF chains

Conclusions

This work utilized LS, OMP, CoSAMP, and DL neural network for estimating millimeter wave channel in millimeter wave cellular system whose receiver has ADC with 2, 3, 4, and 6 bit, respectively, as well few RF chains at both the transmitter and the receiver. Numerical results for normalized mean square error revealed that LS exhibited the worst performance across SNR regime of − 20 to 20 dB except when number of RF chains was 10 with SNR of 6 dB and above.

It was however found that CoSAMP and DL exhibited better performance than OMP in noisy SNR regime of − 30 to − 5 dB, while above − 5 dB, OMP exhibited the best performance. It was found that uniform mid quantizer with 4 bit at SNR of − 10 dB and 6 bit at SNR of 20 dB produce similar results with infinite bit.

It was also observed that DL has the highest spectral efficiency when the number of RF chains at MS and BS was 4, while the spectral efficiency of OMP outperformed others when RF chain was more than 4. It was observed that the spectral efficiency of DL outperformed others when 4 and 6 channel paths were utilized, while OMP had highest spectral efficiency when 8 and 10 channel paths were employed.

In addition, DL compared favorably well with ACS method in the literature, while OMP and CoSAMP performed better than ACS, suggesting that OMP and CoSAMP were better channel estimation tools than ACS. Finally, it was seen that DL, OMP, and CoSAMP have computational advantage over ACS and LS.

Abbreviations

ADC	Analog-to-digital converter
ACS	Adaptive compressed sensing
AoA	Angle of arrival
AoD	Angle of departure
AWGN	Additive white Gaussian noise
BS	Base station
CoSAMP	Compressed sampling matching pursuit
DAC	Digital-to-analog converter
DL	Deep learning
EM	Expectation-maximization
GAMP	Generalized approximate passing
LS	Least square
MIMO	Multiple input multiple output
MS	Mobile station
NMSE	Normalized mean square error
OMP	Orthogonal matching pursuit
RF	Radio frequency
SNR	Signal-to-noise ratio
SURE	Stein's unbiased risk estimate

Acknowledgements

Not applicable.

Authors' contributions

Conceptualization, methodology, investigation, and writing—original draft were done by A. A. R and supervision, investigation, and review by J.F. O, K. A. A, and I.A. A. All authors have read and approved the manuscript.

Funding

Authors do not receive funding from any organization for the work.

Availability of data and materials

All data generated and analyzed have been presented in the body of the work.

Declarations

Competing interests

The authors declare that they have no competing interests.

Received: 4 October 2023 Accepted: 26 January 2024
Published online: 12 February 2024

References

1. Liao A, Gao Z, Wu Y, Wang H, Alouini M-S (2017) 2D unitary ESPIRIT based super-resolution channel estimation for millimeter wave massive MIMO with hybrid precoding. IEEE Access 51:24747–24757. https://doi.org/10.1109/ACCESS.2017.2768579

2. Mendez Rial R, Rusu C, Gonzalez-Preclic N, Alkhateeb A, Heath R-W (2016) Hybrid MIMO architectures for millimeter wave communications: phase shifters or switches. IEEE Access 4:247–267. https://doi.org/10.1109/ACCESS.2015.2514261
3. Rusu C, Mendez-Rial R, Gonzalez –Prelcic N, Heath R-W (2015) Low complexity hybrid sparse precoding and combining in millimeter wave MIMO systems. Proceeding of IEEE ICC 2015 SAC-millimeter wave communications, p. 1340–1345. https://doi.org/10.1109/ICC.2015.7248509
4. Alkhateeb A, Leus G, Heath R-W (2015) Compressed sensing based multi user millimeter wave systems: how many measurements are needed? Proceeding of 2015 IEEE international conference on Acoustics, Speech and Signal Processing (ICASSP), South Brisbane, QLD, Australia, p. 2909–2913.https://doi.org/10.1109/ICASSP.2015.7178503
5. Lee J, Gil GT, Lee Y-H (2014) Exploiting spatial sparsity for estimating channels of hybrid MIMO systems in millimeter wave communications. Proceeding of 2014 IEEE Global communications conference, Texas, USA, p. 3326–3331. https://doi.org/10.1109/GLOCOM.2014.7037320
6. Lee J, Gil GT, Lee Y-H (2016) Channel estimation via orthogonal matching pursuit for hybrid MIMO systems in millimeter wave communications. IEEE Trans Commun 64(6):2370–2386. https://doi.org/10.1109/TCOMM.2016.2557791
7. Huang H, Song Y (2019) Deep-learning based millimeter-wave massive MIMO for hybrid precoding. IEEE Trans Veh Technol 68(3):3027–3032. https://doi.org/10.1109/TVT.2019.2893928
8. Elbir A-M (2019) CNN-based precoder and combiner design in mmWave MIMO system. IEEE Commun Lett 23(7):1240–1243. https://doi.org/10.1109/LCOMM.2019.2915977
9. Venugopal K, Alkhateeb A, Gonzalez-Preclic NN, Heath R-W (2017) Channel estimation for hybrid architecture based wideband millimeter wave systems. IEEE J Select Areas Commun 35(9):1996–2009. https://doi.org/10.1109/JSAC.2017.2720856
10. Schniter P, Sayeed A (2014) Channel estimation and precoder design for millimeter wave communication: the sparse way Proceedings of 2014 IEEE Asilomar Conference on Signals, Systems and Computers, p. 273–277. https://doi.org/10.1109/ACSSC.2014.7094443
11. Heath RW, Gonzalez-Prelcic N, Ragan S, Roh W, Sayeed A (2016) An overview of signal processing techniques for millimeter wave MIMO systems. IEEE J Select Topics Signal Process 10(3):436–453. https://doi.org/10.1109/JSTP.2016.2523924
12. Jacobsen S, Durisi G, Coldrey M, Gustavsson U, Studer C (2015) One- bit massive MIMO channel estimation and high-order modulation. Proceedings of 2015 IEEE International Conference on Communication Workshop (ICCC), 2015. https://doi.org/10.1109/ICCW.2015.7247358
13. Choi J, Mo J, Heath R-W (2016) Near maximum-likelihood detector and channel estimation for Uplink multiuser massive MIMO systems with one-bit ADCs. IEEE Trans Commun 64(5):2005–2018. https://doi.org/10.1109/TCOMM.2016.2545666
14. Stocle C, Munir J, Mezghani A, Nossek JA (2016) Channel estimation in massive MIMO systems using 1-bit quantization. Proceedings of 2016 IEEE 17th International workshop on Signal Processing Advances in Wireless Communication (SPAWC). https://doi.org/10.1109/SPAWC.2016.7536730
15. Li Y, Tao C, Seco-Granados G, Mezghani A, Swindlehurst AL (2017) Channel estimation and performance analysis of one-bit massive MIMO system. IEEE Trans Signal Process 65(5):1–14. https://doi.org/10.1109/TSP.2017.2706179
16. Mo J, Schniter P, Prelcic N-G, Heath R-W (2014) Channel estimation in millimeter wave MIMO systems with one-bit quantization. Proceedings of 2014 48th IEEE Asilomar Conference on Signals, Systems and Computers, 02–05 November, Pacific Groove, USA. https://doi.org/10.1109/ACSSC.2014.7094595
17. Mo J, Alkhateeb A, Abu-Surra S, Heath R-W (2017) Hybrid architectures with few ADC receivers: achievable rates and energy rate consumption. IEEE Trans Wireless Commun 16(14):2274–22874. https://doi.org/10.1109/TWC.2017.2661749
18. Kaushik A, Vlachos E, Thompson J, Perelli A (2018) Efficient channel estimation in millimeter wave MIMO systems with low resolution ADCs. Proceedings of 2018 26th European Signal Processing Conference (EUSIPCO). https://doi.org/10.23919/EUSIPCO.2018.8553303
19. Rusu C, Gonzalez-Prelcic N, Heath R-W (2015) Low resolution adaptive compressed sensing for mmwave MIMO receivers. Proceedings of 2015 49th Asilomar Conference on Signals, Systems and Computers, Pacific Grove, USA, p. 1138–1143. https://doi.org/10.1109/ACSSC.2015.7421318
20. Rao S, Seco-Granados G, Pirzadeh H, Nossek JA, Swindlehurst AL (2021) Massive MIMO channel estimation with low-resolution spatial sigma-delta ADCs. IEEE Access 9(2021):109320–1093344. https://doi.org/10.1109/ACCESS.2021.3101159
21. Prasobh Sankar RS, Chepuri SP (2021) Millimeter wave MIMO channel estimation with 1-bit spatial sigma-delta analog to digital converters. Proceedings of 2021 IEEE International conference on Acoustics, Speech and Signal Processing (ICASSP), p. 4810–4814. https://doi.org/10.1109/ICASSP39728.2021.9414010
22. Samimi MK, Rappaport TS (2016) 3-D Millimeter-wave statistical channel model for 5G wireless system design. IEEE Trans Microw Theory Tech 64(7):2207–2225
23. Alkhateeb A, Ayach OE, Leus G, Heath R-W (2014) Channel estimation and hybrid precoding for millimeter-wave cellular systems. IEEE J Select Topics Signal Process 8(5):831–846. https://doi.org/10.1109/JSTSP.2014.2334278
24. Xiao M, Mumtaz S, Huang Y, Dai L, Li Y, Matthaiou M, Karagiannidis GK, Bjornson E, Yang K, Chin-Chin I, Ghosh A (2017) Millimeter wave communications for future mobile networks. IEEE J Select Areas Commun 35(9):1909–1935. https://doi.org/10.1109/JSAC.2017.2719924
25. Raji AA (2023) Modelling and analysis of low resolution millimeter wave architecture. Unpublished Doctoral Dissertation, Federal University of Agriculture, Abeokuta
26. Ma W, Qi C, Zhang Z, Cheng J (2019) Deep learning for compressed sensing based channel estimation in millimeter wave massive MIMO. Proceedings of 2019 11th International Conference on Wireless Communications and Signal Processing (WCSP). https://doi.org/10.1109/WCSP.2019.8928030

27. Ayach O, Rajagopal S, Abu-Surra S, Pi Z, Heath RW (2014) Spatially sparse precoding in millimeter MIMO systems. IEEE Trans Wireless Commun 13(3):1499–1513. https://doi.org/10.1109/TWC.2014.011714.130846
28. Adaptive Compressed sensing simulation code. http://www.aalkhateeb.net/publications.html?i=1, retrieved January 15, 2023
29. Alkhateeb A, ElAyach O, Leus G, Heath R-W (2014) Channel estimation and hybrid precoding for millimeter wave systems. IEEE J Select Topics Signal Process 8(5):831–846. https://doi.org/10.1109/JSTP.2014.2334278

Publisher's Note